RSC Advances

PAPER

View Article Online
View Journal | View Issue

Check for updates

Cite this: *RSC Adv.*, 2021, **11**, 14787

Rationally designed structure of mesoporous carbon hollow microspheres to acquire excellent microwave absorption performance†

Yuxuan Qin,[a] Muqun Wang,[a] Wei Gao *[ab] and Shaofeng Liang[a]

Received 19th January 2021
Accepted 25th March 2021

DOI: 10.1039/d1ra00465d

rsc.li/rsc-advances

In this study, we used a novel and facile hard-template etching method to manufacture mesoporous carbon hollow microspheres (MCHMs). We prove that the dielectric ability and microwave absorption of MCHMs can be adjusted by structural characteristics. When the average particle size of MCHMs is 452 nm, the paraffin composite material mixed with 10 wt% MCHMs can achieve a maximum reflection loss value of −51 dB with a thickness of 4.0 mm at 7.59 GHz. When the average particle size of MCHMs is 425 nm, the effective absorption bandwidth of the paraffin composite material mixed with 10 wt% MCHMs can achieve a broad bandwidth of 7.14 GHz with a thickness of 2.5 mm. Compared with other microwave absorbers, MCHMs possess high microwave absorption capacity and broad microwave absorption bandwidth with as low as a 10 wt% filler ratio. This excellent microwave absorption performance is due to the internal cavity and the mesoporous shell of MCHMs. By rationally designing the structure of MCHMs, excellent microwave absorption performance can be acquired. Meanwhile, this design concept based on a rational design of spherical structure can be extended to other spherical absorbers.

Introduction

With the rapid development of modern technology, the electromagnetic wave has seriously influenced daily life. Electromagnetic pollution not only affects daily communications but may also be harmful to health.[1–3] Electromagnetic radiation can affect people's nervous system, accompanied by symptoms such as dizziness, headache, insomnia, and memory loss. Severe changes will cause blood, lymph fluid and cell cytoplasm to change, thereby destroying the body's immune system and affecting people's reproduction and metabolism. At the same time, the use of civilian and military electronic products has increased significantly. Electromagnetic interference will cause certain hazards to the stability of electronic products during transportation and storage. Electromagnetic interference not only affects the normal use of electronic products (for example: causing information distortion, functional failure, *etc.*), but also can cause non-negligible damage to the internal components of electronic products. Nevertheless, the current lifestyle requires electromagnetic energy for various complex and miniaturized devices, such as the base station of 5G equipment.[4] As a result, the research of efficient microwave absorber materials is urgent.

The dominating requirements of ideal microwave absorbers are wider absorption bandwidth with good absorption properties, ultrathin structures, and lightweight.[5–8] What is more, the desired microwave absorber can be used in practice at low cost and be easy to fabricate. Recently, there have been numerous research studies about microwave absorbers, including magnetic-based nanomaterials (magnetic alloys, magnetic metals, and magnetic oxides),[9–15] carbon-based nanomaterials (carbon nanotubes, graphene carbon fiber, and porous carbon),[6,16–24] and other special nanomaterials.[25–39] Magnetic-based nanomaterials, such as CoNi particles, have become one of the best choices of microwave absorbers on account of their unique ferromagnetic features. These features contain high magnetocrystalline anisotropy, high saturation magnetization, and high Snoek's limit.[14] Nevertheless, the above materials, except for carbon-based nanomaterials usually possess high density and poor resistance to chemical corrosion, leading to severe limitations to their daily practical applications. Conversely, carbon-based materials are expected to become applicable microwave absorbers on account of their low density, stable chemical properties, tunable structural characteristics, and low cost. Carbon materials are generally used to make up core/yolk–shell structure composites to strengthen dielectric loss ability and lessen integral density. Many studies that focus on rational nanostructures to get ideal microwave absorbers were reported.[39,40] For instance, Liu *et al.* construct yolk–shell structured Co–C/void/Co_9S_8 that composites achieved well microwave absorption with tunable sphere nanostructures.[41] However, when the material is in an environment higher than the Curie temperature, the magnetic particles will lose their magnetism. Carbon

---

[a] *School of Resources, Environment and Materials, Guangxi University, Nanning 530000, Guangxi, China. E-mail: galaxy@gxu.edu.cn*

[b] *Guangxi Engineering and Technology Research Center for High Quality Structural Panels from Biomass Wastes, Nanning 530000, Guangxi, China*

† Electronic supplementary information (ESI) available. See DOI: 10.1039/d1ra00465d

constituent is proven to strengthen microwave attenuation ability by Lv *et al.*[42] It is necessary to design carbon-based spheres microwave absorbers. Carbon-based spheres involve yolk–shell carbon spheres,[14,21] hollow carbon spheres,[43] and mesoporous carbon hollow spheres.[44] Xu *et al.* also produced three kinds of carbon spheres with different structures. In the research, the structure of the carbon spheres including the interior void and mesoporous shell had a significant impact on dielectric loss and impedance matching. The mesosphere hollow spheres showed better microwave absorption than solid carbon spheres and carbon hollow spheres.[45] A large number of methods for preparing hollow structure carbon spheres had emerged.[46–48] In practical applications, a simple and easy-to-operate strategy is requesting for manufacture. In this study, a facile hard-template etching process was used to prepare mesoporous carbon hollow microspheres, which can be applied in actual production on a large scale. The inner and outer diameter of the carbon sphere and the shell thickness can be altered by the additional amount of resorcinol and formaldehyde to regulate the complex permittivity parameters. Compared with other methods that have been reported, the method in this article is simple and easy to implement. At the same time, the fill ratio can still reach the maximum reflection loss of −51 dB even when the fill ratio is reduced to 10 wt%. This provides a novel idea for designing lightweight and efficient microwave absorbers. Our researches would seem to provide a novel thought for the design of microwave absorbers.

Experimental

Chemicals and materials

Concentrated ammonia aqueous solution ($NH_3 \cdot H_2O$, 25%), hydrofluoric acid (HF, 25%), resorcinol, formaldehyde (37%), tetraethyl orthosilicate (TEOS), and absolute ethanol (EtOH) were of analytical grade. All chemical was purchased by Aladdin Company.

Preparation of MCHMs

The schematic graph of the synthesis process of MCHMs was exhibited in Fig. 1. (1) At stage 1, we manufactured colloidal silica spheres by a method of the hard template. 1 mol TEOS was added into the solution involving 40 ml ethanol, 8 ml deionized water, and 3 ml $NH_3 \cdot H_2O$. Then, the solution was kept magnetic stirring for 20 min at indoor temperature. (2) At stage 2, 0.1 mol formaldehyde and 1.92 mmol resorcinol were added into the previous solution while stirring for 8 h. During this stage, the molar ratio of formaldehyde to resorcinol remains constant. The corresponding samples were prepared by the various amount of formaldehyde (0.15 mol, 0.2 mol, 0.25 mol, 0.3 mol) named after P2, P3, P4, P5. (3) At stage 3, $SiO_2@SiO_2$/phenolic resin was centrifuged and washed several times through ethanol and deionized water. Afterward, the sediment was dried in a vacuum oven for 12 h at 60 °C. (4) At stage 4, the compounds were heated for 6 h under an N_2 atmosphere at 700 °C. (5) Finally, $SiO_2@SiO_2$/carbon was etched by HF (25%) for removing the silica scaffold. Furthermore, the filler content of 25% for P3 was investigated, which was named after P3-25 wt%.

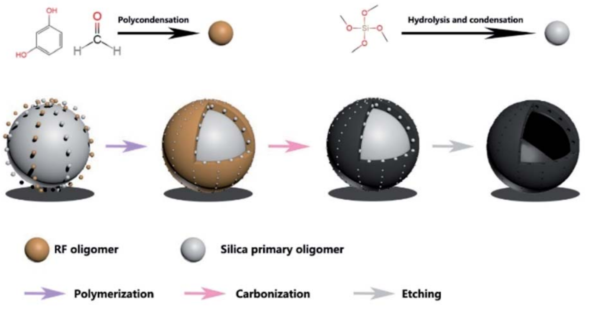

Fig. 1 The diagram of synthesis of samples.

Characterization

The morphology of samples was investigated by a Hitachi SU800 type scanning electron microscope and an FEI Tecnai G2 F20 transmission electron microscopy. The average diameter of the samples was calculated from SEM micrographs using Nano measure software. The automatic specific surface area analyzer (ASAP 2460) was applied to ascertain the Brunauer–Emmett–Teller (BET) specific surface areas and the pore diameter distribution. And the pore diameter distribution of the samples was calculated by the BJH method. The phase structure of MCHMs was ascertained by a Rigaku D/MAX 2500 V X-ray diffractometer with a scanning scope of 10–90°. The degree of graphitization about the carbon of the samples was ascertained by the Raman spectrum (Renishaw inVia). The microwave absorption of samples was tested by testing the electromagnetic parameters with the Agilent PNA N5244A vector network analyzer under the coaxial-line method with the frequency ranges from 2 GHz to 18 GHz. To avoid agglomeration, MCHMs and paraffin wax were added to a solution of hexane with ultrasonic dispersion. The MCHMs were blended with paraffin wax (MCHMs:paraffin wax = 1 : 9) to form a coaxial ring ($F_{\mathrm{in}\frac{1}{4}} =$ 3.04 mm, $F_{\mathrm{out}\frac{1}{4}} = 7.0$ mm).

Results and discussion

As displayed in Fig. 1, the synthesis procedure of MCHMs is grouped into three steps. Firstly, TEOS was hydrolyzed into silica particles in an alkaline solution. Secondly, with the addition of resorcinol and formaldehyde, they accumulated in RF (resorcinol–formaldehyde). As the reaction progresses, the remaining silica particles and RF reacted and condensed on the original SiO_2 core to form a $SiO_2@SiO_2$/RF core–shell structure. Thirdly, $SiO_2@SiO_2$/RF was carbonized at 700 °C to form $SiO_2@SiO_2$/C. Finally, MCHMs were acquired by etching the hard template with HF aqueous.

Fig. 2 show the morphology and structure of P1–P5. The mass ratio between resorcinol and formaldehyde is fixed, our discussion is based on the addition of formaldehyde. When the amount of formaldehyde is 0.1 mol, Fig. 2(a) shows SEM images of P1. It can be seen that there are a lot of broken spheres and hollow hemispheres instead of hollow mesosphere due to the insufficient addition of formaldehyde and resorcinol. As shown in Fig. 2(f), the shell thickness of P1 is only 10 nm. After the SiO_2

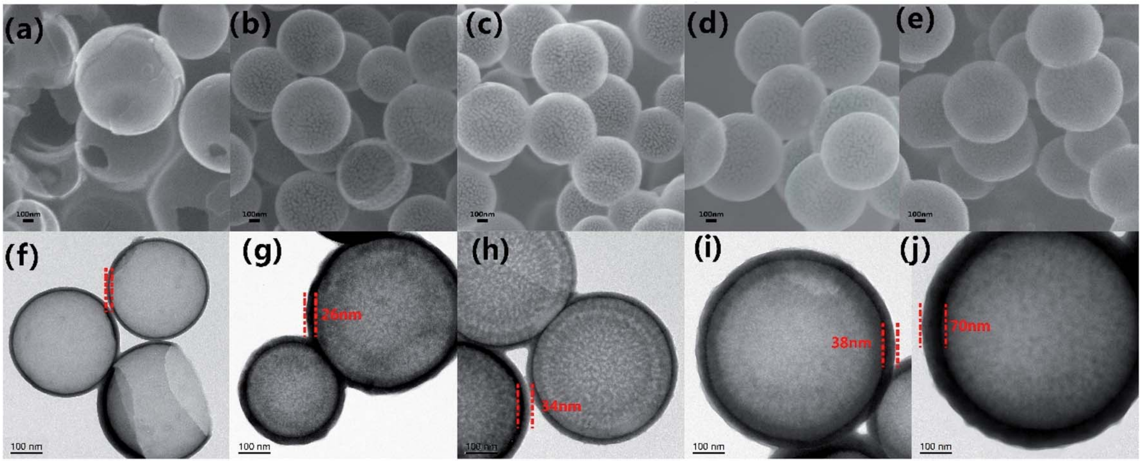

Fig. 2 SEM images of samples P-1 (a), P-2 (b), P-3 (c), P-4 (d), and P-5 (e); TEM images of samples P-1 (f), P-2 (g), P-3 (h), P-4 (i), and P-5 (j); the scale bar is 100 nm.

core is formed, there is no way to interact with it. The remaining SiO_2 forms sufficient SiO_2/SiO_2/RF copolymer on the SiO_2 core. It can be seen form the SEM of Fig. 2(b–e) that the addition of formaldehyde increases from 0.1 mol to 0.15 mol, 0.2 mol, 0.25 mol, 0.3 mol P2–P5 has emerged as a sphere. Compared with P1, P2–P5 have a rough surface. Through measurement and calculation, the average particle size of P2–P5 was 425 nm, 452 nm, 520 nm, 524 nm. The average diameter showed an increasing trend. Through measurement and calculation, the average particle size of P2–P5 was 425 nm, 452 nm, 520 nm, 524 nm. The average diameter showed an increasing trend. TEM images can be seen from Fig. 2(g–j). It can be seen that with the addition of formaldehyde and resorcinol increasing, the shell thickness of P2–P5 was 26 nm, 34 nm, 38 nm and 70 nm. And it showed an increasing trend. The above conclusion showed that the structure of MCHMs could be controlled by changing the content of formaldehyde and resorcinol. As shown in Fig. 2(e), it can be seen that the size distribution of P5 is uneven, which may lead to inhomogeneous distribution in the paraffin matrix.[49]

For carbon-based microwave absorbers, the phase composition and atomic bonding state of carbon atoms will affect the defects and functional groups of the material. The defects and functional groups will cause microwave loss and affect the microwave absorption properties of the material.[50] Therefore, Raman spectroscopy and XRD analysis were executed. It can be seen in Fig. S1 (ESI)† that P1–P5 exhibits a similar broad peak centered at about 22.4° corresponding to the characteristic planes (002) of graphitic carbons.[51] Besides, there is also a very weak peak at 44.2°, which may be attributed to the formation of tiny crystalline domains at the surface of carbon materials.[52] Meanwhile, the degree of graphitization of the samples also impacts the microwave absorption performance of carbon-based microwave absorbers. Raman spectroscopy analysis was used to characterize the degree of graphitization. It can be seen from Fig. 3 that P1–P5 displayed two prominent peaks near 1330 cm^{-1} and 1590 cm^{-1}, which correspond to the D band and the G band, respectively.[53] The D band is a Brinell symmetric breathing mode that contains phonons near the K boundary of the Brillouin zone. The phonons exist in disordered and nanocrystalline graphite. The G band is induced by the sp^2 hybridization of carbon atoms. For carbon materials, a higher carbonization temperature (700 °C) can cause a high degree of graphitization. The value of I_D/I_G is generally applied to depict the degree of graphitization. At the same time, a high graphitization degree usually leads to a good microwave absorption performance.[54] It can be seen from the diagram that the I_D/I_G values P1 to P5 are 0.85, 0.89, 0.90, 0.91, 0.93, respectively. These values show a high degree of similarity, which means these samples have a semblable carbon atom bonding state.

The N_2 adsorption–desorption isotherms were used to display the specific surface area and pore size distribution of MCHMs. The specific surface area of MCHMs was measured by the BET method. With the increase of formaldehyde and resorcinol, the specific surface area of P1–P5 was 440.6 $m^2\ g^{-1}$, 1208.2 $m^2\ g^{-1}$, 1064.5 $m^2\ g^{-1}$, 957.7 $m^2\ g^{-1}$, and 757.7 $m^2\ g^{-1}$. Except P1, the specific surface area decreased with the increase of formaldehyde and resorcinol. And the sample P2 and P3 presented higher specific surface area than other samples, which is related to the damage of agglomeration and hollow features. The microwave absorption performance of

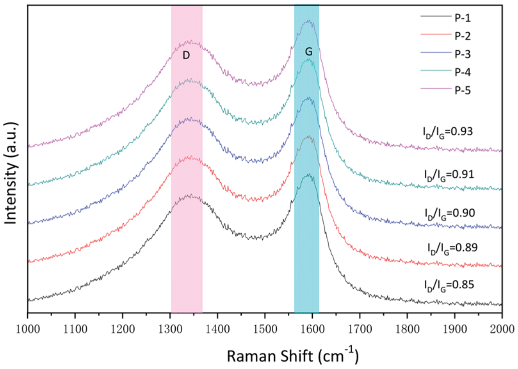

Fig. 3 Raman spectra of samples P-1 to P-5.

carbonaceous materials is related to the specific surface area. The high specific surface area of materials generally enhances the reflection of microwaves and promotes the absorption of microwaves which causes excellent microwave absorption performance.[55] The BJH method was used to calculate the adsorption isotherm curve and pore size distribution.[56] As shown in Fig. S2 (ESI),† the four curves all were long and narrow rings. Monolayer adsorption occurs under low relative pressure, and saturation is reached at the inflection point as the pressure increases. As the pressure continues to increase, multi-layer adsorption and capillary condensation occur. When the capillary agglomeration is over, the largest pore is also filled with agglomeration liquid, and a termination platform appears. At this time, the adsorption capacity has reached the maximum and no further adsorption will occur. According to the IUPAC classification, it is a type IV isotherm adsorption curve which often used to describe mesoporous materials. Fig. 4 showed the diagram of pore intensity distribution when the addition of formaldehyde reaches 0.25 mol and 0.3 mol, and the number of pores is less than the previous 0.1 mol and 0.15 mol. The average pore size of P2–P5 is about 3.1 nm, 3.2 nm, 3.4 nm, 3.6 nm. It further showed that MCHMs exhibited mesopore structures, and P2–P5 expressed similar pore size. In the process of forming hollow mesoporous carbon, a part of the primary silica particles formed by RF acted as SiO_2 core, and the other part of the primary silica particles acted as templates for pores. With the increase in the amount of resorcinol and formaldehyde, it was easier to aggregate and form SiO_2 core during the reaction. That is to say, compared with P2 and P3, during the formation of P4 and P5, most of the primary silica particles formed SiO_2 core, and fewer primary silica particles formed pore templates. As a result, the number of pores decreased. Compared with P4 and P5, P2 and P3 have a smaller inner diameter and a larger number of pores, so they have a higher specific surface area. Because the high specific surface area and a large number of pores are conducive to the incidence of microwaves into the material, which is conducive to the impedance matching. This is one of the most effective ways to expand the effective absorption bandwidth. At the same time, due to the existence of hollow structures and mesopores, the transmission path of incident microwaves will be extended, which will cause multiple scattering of microwaves.[57] As a result, the mesoporous structure is conducive to reflection loss. Incident waves are not only reflected and scattered in the hollow structure of the spheres but also reflected and scattered in the mesopore of the spheres. Both hollow structure and mesoporous structure are very beneficial to microwave absorption.

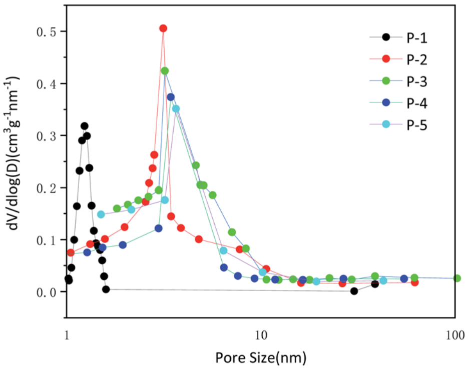

Fig. 4 Pore size distribution plots of samples P-1 to P-5.

The influence of structure on the microwave absorption can be explored by measuring complex permittivity (ε', ε'') and complex permeability (μ', μ'') of MCHMs at different frequencies. It is universally acknowledged that the real part of the complex permittivity (ε') indicates the storage capacity for electricity, and the imaginary part of the complex permittivity (ε'') indicates the loss of electricity capacity. The real part of the complex permeability (μ') indicates the magnetic storage capacity, and the imaginary part of the complex permeability (μ'') indicates the magnetic loss ability.[58,59] Fig. 5 shows the complex permittivity (ε', ε'') and complex permeability (μ', μ'') of the samples. For all samples, the values of μ' were close to 1, and the values of μ'' were close to 0. The reason can be explained as carbon materials are not magnetic. Therefore, the microwave absorption mechanism of carbon materials, mainly due to dielectric loss instead of a magnetic loss. Due to the insufficient amount of resorcinol and formaldehyde added, P1 could not form a complete hollow sphere. The ε' of P1 ranged from 5.3 to 3.9, and ε'' ranged from 0.5 to 1. Low ε' caused a low dielectric loss, which resulted in low microwave absorption attenuation. The ε' of P2–P5 are in the scope of 4.8–7.2, 6–8, 6–13, 8–18, and the ε'' are in the range of 3.0–4.6, 2.5–3.9, 4.7–13, 7.1–23, respectively. It can be known from Fig. 8 that the tangent loss of P1–P5 increases from 0.2 to 0.8, corresponding to the increase in diameter. With the diameter increased, the ε' and ε'' of the samples presented an increasing trend, which indicated that the complex permittivity of the hollow carbon material could be adjusted by the tunable structure. However, the ε'' is higher than ε' of P5 when the frequency ranges from 2 GHz to 5.3 GHz, which may be due to the inhomogeneous dispersion. When ε'' is higher than ε', it will be harmful to impedance matching. Fig. S4 and S5 (ESI)† shows complex permittivity values and microwave reflection loss values at a different thickness of different frequency of P3-20 wt%. The value of ε'' is in the range of 50–350, which is an abnormal parameter. Under the circumstances, the incident microwave will produce violent eddy currents, resulting in energy overflows towards poor microwave absorption performance.[60] At this moment, the sample/paraffin will form a conductive channel after doping, which exceeds the percolation threshold. The sample is close to the conductor, which only exhibits a microwave shielding effect but not electromagnetic wave absorption performance. Therefore, when designing an efficient microwave wave absorber reasonably, the filler content should be arranged reasonably.

For the sake of evaluating the microwave absorption performance of MCHMs. The reflection loss value (RL) under different matching thicknesses was calculated by the following formula. The calculation is carried out based on the theory of free transmission line with complex permittivity:

$$Z_{\mathrm{in}} = Z_0\sqrt{\frac{\mu_{\mathrm{r}}}{\varepsilon_{\mathrm{r}}}}\tan\left[j\left(\frac{2\pi fd}{c}\right)\sqrt{\mu_{\mathrm{r}}\varepsilon_{\mathrm{r}}}\right] \tag{1}$$

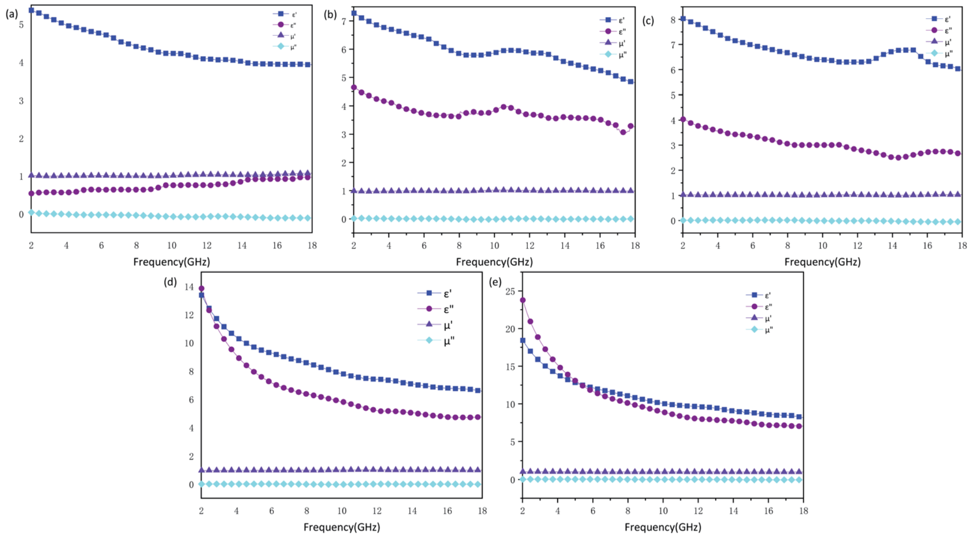

Fig. 5 Complex permittivity and permeability values of samples P-1 (a), P-2 (b), P-3 (c), P-4 (d) and P-5 (e).

$$\mathrm{RL}\ \ (\mathrm{dB}) = 20\log\left|\frac{Z_{\mathrm{in}} - Z_0}{Z_{\mathrm{in}} + Z_0}\right| \quad (2)$$

where Z_{in} refers to the input impedance of the absorber, Z_0 is the impedance of free space, μ_{r} ($\mu_{\mathrm{r}} = \mu' - j\mu''$) and ε_{r} ($\varepsilon_{\mathrm{r}} = \varepsilon' - j\varepsilon''$) is the relative complex permeability and the relative complex permittivity, c is the speed of light in free space, f is the frequency of microwave, and d is the layer thickness of the absorber. The effective absorption bandwidth is RL within −10 dB (90% of microwaves are absorbed). Fig. 6 and 7 show the reflection loss values from 2–18 GHz with matching thickness from 1.0–5.5 mm, and the effective absorption area is marked with a black line. For P1, $\mathrm{RL}_{\mathrm{min}}$ (the value of minimum reflection loss) is −5.02 dB when the thickness is 4.0 mm at 14.6 GHz, which is less than −10 dB. As a result, P1 cannot effectively attenuate the microwave. The $\mathrm{RL}_{\mathrm{min}}$ of P2 can reach −22 dB when the thickness is 2 mm at 17.44 GHz, and the valid bandwidth can achieve a broad bandwidth of 7.14 dB (10.65–17.79 GHz) when the thickness is 2.5 mm.

The $\mathrm{RL}_{\mathrm{min}}$ of P3 reaches −51 dB at 7.59 GHz with a thickness of 4.0 mm when the effective bandwidth of 3.92 GHz (6.2–10.13 GHz). The excellent microwave absorption performance of P2 and P3 is attributed to low dielectric loss and suitable impedance matching performance. When the $\mathrm{RL}_{\mathrm{min}}$ of P4 reaches −14.06 dB at 14 GHz, with a thickness of 2 mm, the valid bandwidth ranges from 12 to 17 GHz is achieved. In terms of P5, only when the matching thickness is 5.5 mm and the microwave frequency is high (15.9–18 GHz), it has effective microwave absorption performance with $\mathrm{RL}_{\mathrm{min}}$ of −10.76 dB at 17.13 GHz. Fig. 7 shows a 2D plot of the reflection loss under different thicknesses. It can also

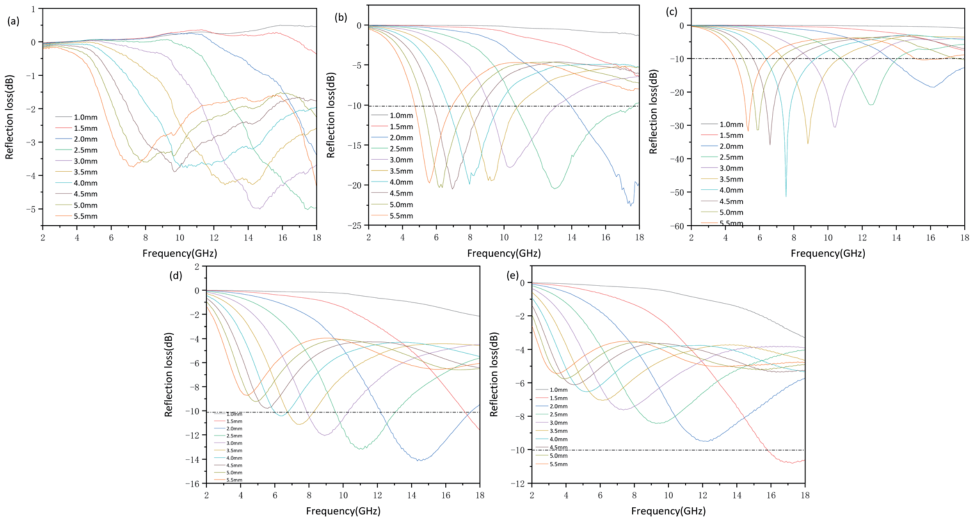

Fig. 6 Microwave reflection loss values at different thickness of different frequency of samples P-1 (a), P-2 (b), P-3 (c), P-4 (d) and P-5 (e).

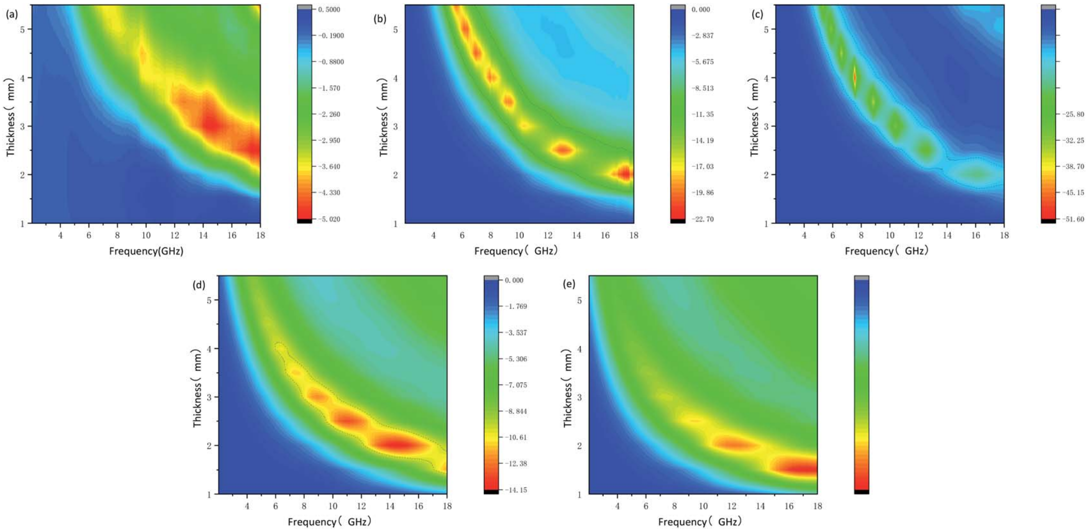

Fig. 7 2D plot of reflection loss values of samples P-1 (a), P-2 (b), P-3 (c), P-4 (d) and P-5 (e).

be seen intuitively that compared with P4 and P5, P2 and P3 have wider effective bandwidth. Therefore, the appropriate complex permittivity of the carbon material leads to the good microwave absorption performance. At the same time, it indicated that whether too much or too little addition of formaldehyde and resorcinol will cause weak microwave absorption performance. Failure to form a complete hollow spherical structure will result in insufficient microwave attenuation. And inhomogeneous dispersity will cause most of the microwave to reflect. The above results declare tunable nanostructures of MCHMs have a significant impact on microwave absorption performance.

On the other hand, the imaginary part of the dielectric constant and the imaginary part of the permeability of the absorptive material determines its ability to attenuate electromagnetic wave losses. The loss factor is usually used to characterize the size of the loss. The loss factor can be divided into electrical loss factor and magnetic loss factor, which respectively represent the capacity of dielectric loss and magnetic loss. The loss factor is the loss tangent value, which can be expressed by the following equation: $\tan\delta_\varepsilon = \varepsilon''/\varepsilon'$, $\tan\delta_\mu = \mu''/\mu'$. Among them, δ_ε is the dielectric loss angle and δ_μ is the magnetic loss angle.[61] There is basically no magnetic loss in carbon materials. The tangent loss value of P1–P5 can be obtained from Fig. 8. The tangent loss value of P1 is 0–0.2, and the tangent loss of P2–P5 increases from 0.4 to 0.8. Theoretically, as the average diameter increases, the tangent loss should appear increasing trend. However, although the diameter of P3 is larger than P2, the tangent loss of P3 is smaller than P2. Generally, the dielectric loss mainly comes from polarization loss and conduction loss. Polarization loss includes dipolar polarization, interface polarization, ion polarization, and electronic polarization. However, ion polarization and electrons generally occur at high frequencies of 103–106 GHz, so the polarization loss of MCHMs is dominated by dipolar polarization and interface polarization. Dipole polarization occurs on molecules with obvious dipole moments, and interface polarization usually occurs in materials composed of more than one phase. Due to the accumulation and uneven distribution of space charges, heterostructures will occur.[62] If there is a cavity in the absorbent material, it may be stronger at the internal interface. It can be seen from Fig. 2 that compared to P3, the distribution of P2 is relatively uneven. Therefore, the higher tangent loss of P2 may be attributed to the stronger polarization loss. Therefore, the enhanced microwave absorption performance may be attributed to the enhanced interface polarization originating from the hollow structure. In MCHMs/paraffin composites, due to the multipole interaction between the incident EM wave and the interface, the multiple interfaces between MCHMs, paraffin wax, and air cavity can improve the microwave absorption performance.[63]

Excellent microwave absorption performance also depends on high attenuation constant α and suitable impedance matching. The attenuation constant of different samples is calculated by the following formula:[64]

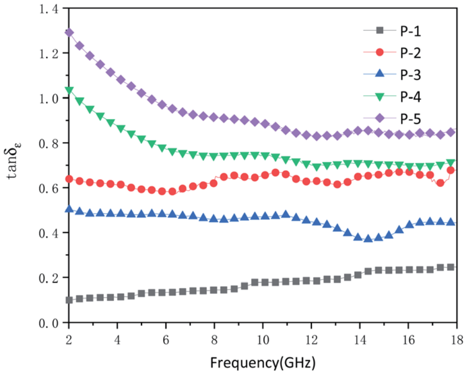

Fig. 8 Dielectric loss tangent factor of samples P-1 to P-5.

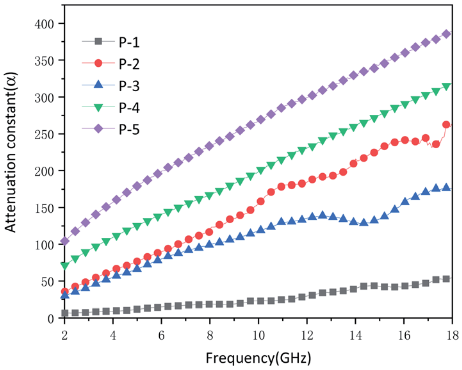

Fig. 9 Attenuation constant of samples P-1 to P-5 *versus* frequency.

$$\alpha = \frac{\sqrt{2}\pi f}{c} \times \sqrt{\sqrt{(\mu''\varepsilon'' - \mu'\varepsilon')} + \sqrt{(\mu''\varepsilon'' - \mu'\varepsilon')^2 + (\mu'\varepsilon'' + \mu''\varepsilon')^2}} \tag{3}$$

It can be seen from Fig. 9 that the attenuation constant of P1 ranges from 6.767 to 54.479. A low attenuation constant cannot effectively attenuate the microwave. P2–P5 all had a high attenuation constant, which was relevant to the effective microwave absorption performance. It was ascribed to the porous hollow mesosphere structure, while P1 cannot effectively absorb microwave. P2 and P3 had semblable attenuation constants on account of similar nanostructures. While the attenuation constants of P4 and P5 will augment with the increase of diameter, which further declared the increase in diameter could strengthen the microwave scattering and reflection in the internal cavity. Excellent microwave absorption performance requires not only high attenuation constant but also good impedance matching. $Z = |Z_{\text{in}}/Z_0|$, Z is generally used to characterize whether it has good impedance matching. While Z is equivalent to or comes near 1, the microwaves are not reflected on the absorbing surface. On the contrary, all microwaves will incident inside the absorbing body.[41] In this situation, the RL will reach the maximum which means the best microwave absorption. In other words, even with high dielectric loss and magnetic loss, the impedances do not match, a majority of the incident microwave will be reflected on or pass through the surface of the absorbing material without any attenuation, which will lead to poor reflection loss. As shown in Fig. S3 (ESI),† the Z of P1 is much higher than 1. The low attenuation constant of P1 and poor impedance matching make it impossible to have effective microwave absorption performance. The Z of P3 hovers around 1. As a consequence, P3 has outstanding microwave absorption performance. The Z of P2 is also close to 1, so it has effective microwave absorption performance. The Z of P4 and P5 range from 0 to 0.5, which has undesirable impedance matching. Although P4 and P5 have higher attenuation constants and lower dielectric loss than P2 and P3, they cannot have higher microwave absorption than P2 and P3. It is necessary to design the nanostructure rationally when devising high-efficiency microwave absorbers.

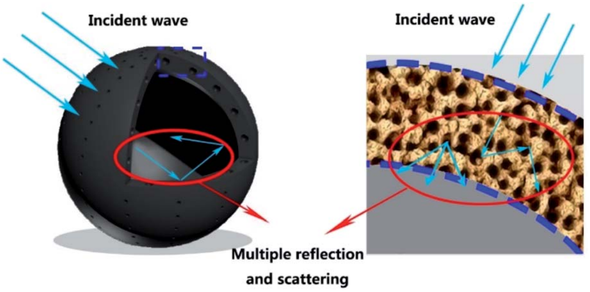

Fig. 10 Schematic illustration of microwave absorption mechanisms for samples.

Fig. 10 shows the microwave absorption mechanism of hollow mesoporous carbon spheres. After the incident microwave has multiple reflections and scattering in the spherical cavity, multiple reflections and scattering will occur again in the mesoporous shell. At the same time, the carbon–air interface helps to enhance the interface polarization to achieve good impedance matching. These two mechanisms make hollow mesoporous carbon materials have good microwave absorption properties. Table 1 shows the microwave absorption performance of different carbon-based materials. Compared with other materials, MCHMs show high microwave absorption and broad effective microwave absorption bandwidth with a lower filler ratio.

Table 1 Microwave absorption performance of the different carbon-based materials

Sample	Filler content (wt%)	Thickness (mm)	RL_{min} (dB)	Bandwidth (GHz)	Ref.
$Co_{15}Fe_{85}$@C/RGO	60	2.5	−33.38	9.2	58
Mesoporous carbon hollow spheres	20	2–3	−38.5	6.2	55
CCNS/Ni	30	1.68	−28.32	4.6	51
SWNTs	5	—	−22	8.8	65
NOMC	70	1.6	−30	K_u-band	66
CF/MXene	9.8	4.5	−45	8.8	29
CoNi@SiO_2@C	50	2.2	−46	5.6	12
P2	10	2	−22	7.14	This work
P3	10	4	−51	3.92	This work

Conclusions

We prepared MCHMs with adjustable properties after forming a hard template by resorcinol and formaldehyde and then etching the silicon. Besides, the different shell thickness and diameter of MCHMs can be obtained by adjusting the addition of phenolic resin. P2 with an average diameter of 420 nm has a maximum reflection loss of −22 dB with a broad effective bandwidth of 7.14 GHz at a thickness of 2 mm, and P3 with an average diameter of 425 nm has a maximum reflection loss of −51 dB with an effective microwave absorption bandwidth of 3.92 GHz at a thickness of 4 mm. The excellent microwave absorption performance of P2 and P3 is mainly due to the suitable impedance matching and low attenuation constant brought by suitable nanostructures. It can be seen that an excellent microwave absorber can be obtained by rationally designing nanostructures.

Author contributions

Yuxuan Qin: conceptualization, data curation, formal analysis, validation, writing-original draft, writing-review & editing. Muqun Wang: writing-review & editing, software. Wei Gao: funding acquisition, resources, supervision. Shaofeng Liang: writing-review & editing, validation.

Conflicts of interest

There are no conflicts to declare.

Acknowledgements

The project is supported by Guangxi University "College Students' Innovation and Entrepreneurship Training Program", Study on Magnetic Wood Porous Activated Carbon Fiber Microwave Adsorbent (201910593216).

Notes and references

1 R. W. Shu, Z. L. Wan, J. B. Zhang, Y. Wu, Y. Liu, J. J. Shi and M. D. Zheng, *ACS Appl. Mater. Interfaces*, 2020, **12**, 4689–4698.

2 Z. Xiang, J. Xiong, B. W. Deng, E. Cui, L. Z. Yu, Q. W. Zeng, K. Pei, R. C. Che and W. Lu, *J. Mater. Chem. C*, 2020, **8**, 2123–2134.

3 M. M. Zhang, Z. Y. Jiang, H. X. Si, X. F. Zhang, C. X. Liu, C. H. Gong, Y. H. Zhang and J. W. Zhang, *Phys. Chem. Chem. Phys.*, 2020, **22**, 8639–8646.

4 X. Yang, Y. P. Duan, Y. S. Zeng, H. F. Pang, G. J. Ma and X. H. Dai, *J. Mater. Chem. C*, 2020, **8**, 1583–1590.

5 H. L. Yang, X. Zhang, Z. Q. Xiong, Z. J. Shen, C. B. Liu and Y. Xie, *Ceram. Int.*, 2021, **47**, 2155–2164.

6 R. Bhattacharyya, V. K. Singh, S. Bhattacharyya, P. Maiti and S. Das, *Appl. Surf. Sci.*, 2021, **537**, 14780.

7 Y. Wang, X. C. Di, X. M. Wu and X. H. Li, *J. Alloys Compd.*, 2020, **846**, 156215.

8 L. X. Huang, Y. P. Duan, X. Yang, S. H. Gao, Y. S. Zeng, G. J. Ma and W. P. Zhang, *Compos. Struct.*, 2019, **229**, 18952–18963.

9 N. Yang, Z. X. Luo, S. C. Chen, G. Wu and Y. Z. Wang, *ACS Appl. Mater. Interfaces*, 2020, **12**, 18952–18963.

10 K. F. Wang, Y. J. Chen, H. Li, B. B. Chen, K. Zeng, Y. L. Chen, H. C. Chen, Q. L. Liu and H. Z. Liu, *ACS Appl. Nano Mater.*, 2019, **2**, 8063–8074.

11 X. J. Zeng, G. M. Jiang, L. Y. Zhu, C. Y. Wang, M. Chen and R. H. Yu, *ACS Appl. Nano Mater.*, 2019, **2**, 5475–5482.

12 S. H. Zhou, Y. Huang, X. D. Liu, J. Yan and X. S. Feng, *Ind. Eng. Chem. Res.*, 2018, **57**, 5507–5516.

13 Y. Liu, Z. Chen, Y. Zhang, R. Feng, X. Chen, C. X. Xiong and L. J. Dong, *ACS Appl. Mater. Interfaces*, 2018, **10**, 13860–13868.

14 N. Chen, J. T. Jiang, C. Y. Xu, S. J. Yan and L. Zhen, *Sci. Rep.*, 2018, **8**, 3196.

15 C. X. Zhang, Y. H. Li, Y. P. Duan and W. Zhang, *J. Magn. Magn. Mater.*, 2020, **497**, 165988.

16 F. Sultanov, C. Daulbayev, B. Bakbolat and O. Daulbayev, *Adv. Colloid Interface Sci.*, 2020, **285**, 102281.

17 Z. H. Li, X. S. Qi, X. Gong, R. Xie, C. Y. Deng and W. Zhong, *Carbon*, 2020, **161**, 685–693.

18 M. S. Saeed, J. Seyed-Yazdi and S. H. Hekmatara, *Chem. Phys. Lett.*, 2020, **756**, 137823.

19 X. Chen, Y. Gu, J. Liang, M. Bai, S. Wang, M. Li and Z. Zhang, *Composites, Part A*, 2020, **139**, 106099.

20 Y. Huangfu, K. Ruan, H. Qiu, Y. Lu, C. Liang, J. Kong and J. Gu, *Composites, Part A*, 2019, **121**, 265–272.

21 Z. Li, X. Han, Y. Ma, D. Liu, Y. Wang, P. Xu, C. Li and Y. Du, *ACS Sustainable Chem. Eng.*, 2018, **6**, 8904–8913.

22 X. Liang, B. Quan, Z. Man, B. Cao, N. Li, C. Wang, G. Ji and T. Yu, *ACS Appl. Mater. Interfaces*, 2019, **11**, 30228–30233.

23 X. Ma, H. Peng, H. Yang and C. Liu, *Chin. Sci. Bull.*, 2019, **64**, 3188–3195.

24 H. Zhang, B. Wang, A. Feng, N. Zhang, Z. Jia, Z. Huang, X. Liu and G. Wu, *Composites, Part B*, 2019, **167**, 690–699.

25 X. F. Liu, X. Y. Nie, R. H. Yu and H. B. Feng, *Chem. Eng. J.*, 2018, **334**, 153–161.

26 X. Li, M. Zhang, W. You, K. Pei, Q. Zeng, Q. Han, Y. Li, H. Cao, X. Liu and R. Che, *ACS Appl. Mater. Interfaces*, 2020, **12**, 18138–18147.

27 K. Rajavel, Y. Hu, P. Zhu, R. Sun and C. Wong, *Chem. Eng. J.*, 2020, **399**, 125791.

28 Z. Song, M. Sun, L. Wu, F. Wu and A. Xie, *Mater. Res. Express*, 2020, **7**(4), 046301.

29 Y. Wang, J. Yang, Z. Chen and Y. Hu, *RSC Adv.*, 2019, **9**, 41038–41049.

30 M. Yang, Y. Yuan, Y. Li, X. Sun, S. Wang, L. Liang, Y. Ning, J. Li, W. Yin and Y. Li, *ACS Appl. Mater. Interfaces*, 2020, **12**, 33128–33138.

31 N. Gao, W.-P. Li, W.-S. Wang, P. Liu, Y.-M. Cui, L. Guo and G.-S. Wang, *ACS Appl. Mater. Interfaces*, 2020, **12**, 14416–14424.

32 B. Huang, Z. Wang, H. Hu, X.-Z. Tang, X. Huang, J. Yue and Y. Wang, *Ceram. Int.*, 2020, **46**, 9303–9310.

33 Q. Li, X. Tian, W. Yang, L. Hou, Y. Li, B. Jiang, X. Wang and Y. Li, *Appl. Surf. Sci.*, 2020, **530**, 147298.

34 L. Lyu, F. Wang, J. Qiao, X. Ding, X. Zhang, D. Xu, W. Liu and J. Liu, *J. Alloys Compd.*, 2020, **817**, 153309.

35 Q. Shang, H. Feng, K. Pan, N. Chen, L. Tan and J. Qiu, *J. Mater. Sci. Mater. Electron.*, 2020, **31**, 8523–8535.

36 X. Sun, X. Yuan, X. Li, L. Li, Q. Song, X. Lv, G. Gu and M. Sui, *New J. Chem.*, 2018, **42**, 6735–6741.

37 Y. Wang, X. Gao, X. Wu and C. Luo, *Ceram. Int.*, 2020, **46**, 1560–1568.

38 L. X. Huang, Y. P. Duan, X. H. Dai, Y. S. Zeng, G. J. Ma, Y. Liu, S. H. Gao and W. P. Zhang, *Small*, 2019, **15**, 40.

39 L. L. Song, Y. P. Duan, J. Liu and H. F. Pang, *Nano Res.*, 2020, **13**, 95–104.

40 M. Gonzalez, M. Crespo, J. Baselga and J. Pozuelo, *Nanoscale*, 2016, **8**, 10724–10730.

41 X. Liu, C. Hao, L. He, C. Yang, Y. Chen, C. Jiang and R. Yu, *Nano Res.*, 2018, **11**, 4182.

42 H. L. Lv, G. B. Ji, W. Liu, H. Q. Zhang and Y. W. Du, *J. Mater. Chem. C*, 2015, **3**, 10232–10241.

43 C. Zhou, S. Geng, X. W. Xu, T. H. Wang, L. Q. Zhang, X. J. Tian, F. Yang, H. T. Yang and Y. F. Li, *Carbon*, 2016, **108**, 234–241.

44 Y. Cheng, Z. Li, Y. Li, S. Dai, G. Ji, H. Zhao, J. Cao and Y. Du, *Carbon*, 2018, **127**, 643–652.

45 H. L. Xu, X. W. Yin, M. Zhu, M. K. Han, Z. X. Hou, X. L. Li, L. T. Zhang and L. F. Cheng, *ACS Appl. Mater. Interfaces*, 2017, **9**, 6332–6341.

46 H. Zhang, B. Wang, A. Feng, N. Zhang, Z. Jia, Z. Huang, X. Liu and G. Wu, *Composites, Part B*, 2019, **167**, 690–699.

47 P. Liu, W. Liu, Y. Huang, P. Li, J. Yan and K. Liu, *Energy storage Materials*, 2020, **25**, 858–865.

48 C. Zhou, S. Geng, X. Xu, T. Wang, L. Zhang, X. Tian, F. Yang, H. Yang and Y. Li, *Carbon*, 2016, **108**, 234–241.

49 B. Quan, W. H. Gu, J. Q. Sheng, X. F. Lv, Y. Y. Mao, L. Liu, X. G. Huang, Z. J. Tian and G. B. Ji, *Nano Res.*, 2020, **14**(5), 1495–1501.

50 X. Yan, X. X. Huang, Z. Bo, W. Tong, H. T. Wang, T. Zhang, N. M. Bai, G. P. Zhou, H. Pan, G. W. Wen and L. Xia, *Chem. Eng. J.*, 2020, **391**, 123538.

51 Z. Gao, C. X. Zhao, Y. Y. Li and Y. L. Yang, *Appl. Microbiol. Biotechnol.*, 2019, **103**(11), 4585–4593.

52 R. Qiang, Y. C. Du, Y. Wang, N. Wang, C. H. Tian, J. Ma, P. Xu and X. J. Han, *Carbon*, 2016, **98**, 599–606.

53 A. C. Ferrari and J. Robertson, *Phys. Rev. B: Condens. Matter Mater. Phys.*, 2000, **61**, 14095–14107.

54 G. L. Wu, Y. H. Cheng, Z. H. Yang, Z. R. Jia, H. J. Wu, L. J. Yang, H. L. Li, P. Z. Guo and H. L. Lv, *Chem. Eng. J.*, 2018, **333**, 519–528.

55 J. B. Chen, X. H. Liang, W. Liu, W. H. Gu, B. S. Zhang and G. B. Ji, *Dalton Trans.*, 2019, **48**, 10145–10150.

56 E. P. Barrett, L. G. Joyner and P. P. Halenda, *J. Am. Chem. Soc.*, 1951, **73**, 380.

57 G. H. He, Y. P. Duan and H. F. Pang, *Nano-Micro Lett.*, 2020, **12**(1), 57.

58 S. S. Bao, W. Tang, Z. J. Song, Q. R. Jiang, Z. Y. Jiang and Z. X. Xie, *Nanoscale*, 2020, **12**, 18790–18799.

59 H. D. Ren, J. L. Ma, J. Zhou, X. F. Shu, Z. Y. Liu, Y. Liu, Y. Zhao, T. Ge, F. F. Min and L. B. Kong, *New J. Chem.*, 2020, **44**, 13962–13970.

60 Y. Cheng, Z. Y. Li, Y. Li, S. S. Dai, G. B. Ji, H. Q. Zhao, J. M. Cao and Y. W. Du, *Carbon*, 2018, **127**, 643–652.

61 X. J. Zeng, X. Y. Cheng, R. H. Yu and G. D. Stucky, *Carbon*, 2020, **168**, 606–623.

62 W. Liu, Q. Shao, G. Ji, X. Liang, Y. Cheng, B. Quan and Y. Du, *Chem. Eng. J.*, 2017, **313**, 734–744.

63 W. She, H. Bi, Z. Wen, Q. Liu, X. Zhao, J. Zhang and R. Che, *ACS Appl. Mater. Interfaces*, 2016, **8**, 9782–9789.

64 X. Wang, Q. Geng, G. Shi, Y. Zhang and D. Li, *CrystEngComm*, 2020, **22**, 6796–6804.

65 Z. F. Liu, G. Bai, Y. Huang, F. F. Li, Y. F. Ma, T. Y. Guo, X. B. He, X. Lin, H. J. Gao and Y. S. Chen, *J. Phys. Chem. C*, 2007, **111**, 13696–13700.

66 G. Z. Shen, Y. W. Xu, B. Liu, P. Du, Y. Li, J. Zhu and D. Zhang, *J. Alloys Compd.*, 2016, **680**, 553–559.